Experimental investigation of the effects of embankment scenario on railway vehicle aerodynamic coefficients

G. Tomasini *, S. Giappino, R. Corradi

Department of Mechanical Engineering, Politecnico di Milano, Milano, Italy

Article history:
Received 21 January 2014
Received in revised form
12 May 2014
Accepted 13 May 2014
Available online 5 June 2014

1. Introduction

The analysis of cross-wind effects on railway vehicles has become, with the development of new high-speed railway lines, one of the main problems in transport safety (Baker et al., 2009). The need for international interoperability standards has brought to the attention of the international scientific community the subject of cross-wind safety. Two international standards for railway vehicles issued in recent years EN 14067-6 (2010) and TSI HS RST (2008), have specific sections on cross-wind safety. The approach to evaluating the cross-wind stability of a railway vehicle described in these two standards, but also in a number of national standards, is based both on the determination of vehicle aerodynamic coefficients using (preferably) wind tunnel tests or CFD calculations, and on the evaluation of the maximum cross-wind speeds at which a vehicle reaches its safety limits, that is the Characteristic Wind Curves (Cheli et al., 2004, 2012; Carrarini, 2007; Sesma et al., 2012; Baker, 2010b; Ding et al., 2008; Diedrichs, 2003; Tomasini and Cheli, 2013).

In particular, in the TSI standard, wind tunnel tests are required for the evaluation of rail vehicle aerodynamic coefficients with two reference scenarios: flat ground and embankment. The flat ground corresponds to the condition of a train running on a flat terrain: this scenario is very simple to reproduce but is not realistic because it does not take into account the effects of infrastructure (ballast, viaduct, etc.) in the evaluation of the aerodynamic coefficients.

The embankment is a typical scenario for railway infrastructures: it represents one of the most critical scenarios owing to the flow acceleration associated with its specific geometry (Bocciolone et al., 2008; Cheli et al., 2010; Diedrichs et al., 2007; Peng and Xiaodong, 2010; Schober et al., 2010). Higher speeds at the top of the scenarios correspond to higher aerodynamic forces on the rail vehicle and, as a consequence, to greater safety risks.

In past years, wind tunnel tests have been carried out to study the topographical effects of the scenario (Baker, 1985) and to

* Corresponding author. Tel.: +39 223998480; fax: +39 223998492.
E-mail address: gisella.tomasini@polimi.it (G. Tomasini).

evaluate the effects of different embankment heights and boundary layer simulation on the flow acting on the train (Suzuki et al., 2003). Beside the experimental investigations using wind tunnel tests, in recent years CFD numerical analyses have also been carried out (Diedrichs et al., 2007; Ekeroth et al., 2009; Catanzaro et al., 2010).

Generally, the experience gained in these first experimental campaigns showed that the modelling of the embankment scenario in wind tunnel had some defects and open points (Cheli et al., 2010; Diedrichs et al., 2007; Suzuki et al., 2003):

- tests with still vehicle models, which do not reproduce the train-infrastructure relative velocity, do not permit correct simulation of the relative velocities train-wind (which should depend on vehicle speed) and infrastructure-wind (corresponding to the true wind speed, since the scenario is immobile also in real conditions);
- the model scale is limited by the need for a blockage ratio lower than 15% (EN 14067-6, 2010), or as lower as 10% (TSI HS RST, 2008) with a consequent reduction of the Reynolds number;
- the flow around the embankment simulated in the wind tunnel is significantly influenced by the unrealistic finite length of the scenario model and by the proximity of the wind tunnel walls, which modify the wind flow around the vehicle compared with real, open field conditions.

As concerns the first point, CFD numerical studies were performed to evaluate the effects of non-moving model tests on aerodynamic coefficients (Cheli et al., 2011c): these analyses showed that this effect, with the train set on the embankment infrastructure scenario, modifies of about 10% the lateral force and rolling moment coefficients, in the range of wind angle up to 30° (upwind and downwind) and of about 15% the vertical force coefficient. On the second point, the effects of the Reynolds number on vehicle aerodynamic coefficients have been studied by a number of researchers (Bocciolone et al., 2008; Cheli et al., 2011d; Baker, 1991) also comparing train coefficients measured in wind tunnel and on field at real scale (Baker et al., 2004); anyway, Reynolds number effects specifically with the embankment scenario are less studied (Schober et al., 2010). Finally, on the need to use noses at the ends of infrastructure models, tests have been conducted in Schober et al. (2010) and, for the viaduct, in Cheli et al. (2010). This paper deals with the analysis of the effects of embankment modelling on the evaluation of force and pressure aerodynamic coefficients of railway vehicles using wind tunnel tests on scale models. The aim of the research is to investigate different methods of performing wind tunnel tests with the embankment scenario and to propose a critical analysis of the TSI standard as regards the adequacy of the technical requirements it contains and, in general, the advisability of adopting the embankment as the reference scenario.

In particular, three main topics are analysed in this work:

1. the effects of Reynolds number in the range [$Re = 4 \times 10^4 - Re = 2.2 \times 10^5$];
2. the effect of different embankment reproductions (with different end layouts);
3. the sensitivity of the coefficients to the distance of the vehicle model from the wind tunnel walls (wall proximity effects).

To study the three topics, two wind tunnel experimental campaigns were carried out with a 1:45 scale ETR500 train model on the 6 m-high embankment described in the TSI standard, with wind speeds from 10 to 52 m/s ($Re_{max} = 2.2 \times 10^5$). In the first tests, performed in a 1.5×1 m wide wind tunnel section, two end layout conditions were simulated: a finite length embankment, with end-noses having different slopes, and a "pseudo-infinite" embankment, reproduced by wall-to-wall extension of the scenario. This is considered as the reference configuration because it represents the model most similar to the real infinite length embankment condition. Two different vehicle models were designed for the measurement of, respectively, aerodynamic forces and surface pressures. The final goal of this first campaign was to verify the minimum length of the embankment needed to obtain results equivalent, in terms of aerodynamic coefficients, to the ones found for the wall-to-wall configuration and to test different end-elements (noses) for the embankment.

The second experimental campaign was then performed in a wider wind tunnel section (4×4 m), with a greater distance between the vehicle ends and the wind tunnel walls. Moreover, in order to understand the effects of wall proximity, the results of the two experimental campaigns were compared with the reference data for the ETR500 train reported in EN 14067-6, obtained in a previous wind tunnel test carried out in the Boundary Layer Test Section of Politecnico di Milano (14×4 m wide) on a 1:10 scale model (Cheli et al., 2010). In particular, Section 2 focuses on the description of the wind tunnel experimental set-up while Section 3 describes the results of the two experimental campaigns.

2. Wind tunnel tests: Experimental set-up

All the tests described in this paper are compliant with the international standards (EN 14067-6, 2010; TSI HS RST, 2008).

Tests were carried out in two wind tunnels having different test section dimensions:

- A 1.5×1 m section of the Politecnico di Milano Aerospace Science and Technology department wind tunnel (hereafter named DIA section);
- A 4×4 m section of the Politecnico di Milano CIRIVE wind tunnel (hereafter CIRIVE1 section).

In addition, the force coefficients will also be compared with the reference coefficients for the ETR500 train reported in the EN 14067-6 standard (Table E.12). The tests to obtain these coefficients were performed in the Politecnico di Milano wind tunnel boundary layer test section (hereafter CIRIVE2) and are described in Cheli et al. (2010).

This data set was measured on a 1:10 scale ETR500 model positioned on a 6 m high standard embankment (Fig. 1). In this case the scenario had a fixed length of 130 m full scale (45° skewed end noses were adopted for yaw angles up to 20°, see Fig. 4) and the distance between power car and the test section wall was about 50 m full scale (at all yaw angles). At a 30° wind angle the blockage ratio was about 14%. All the three wind tunnels have a fully enclosed test section.

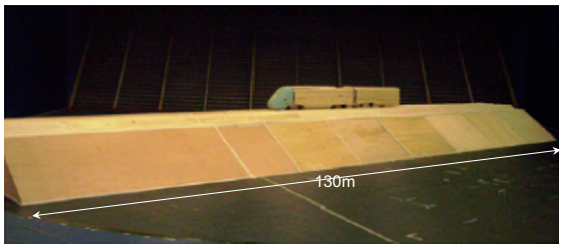

Fig. 1. CIRIVE2, boundary layer test section (model scale 1:10).

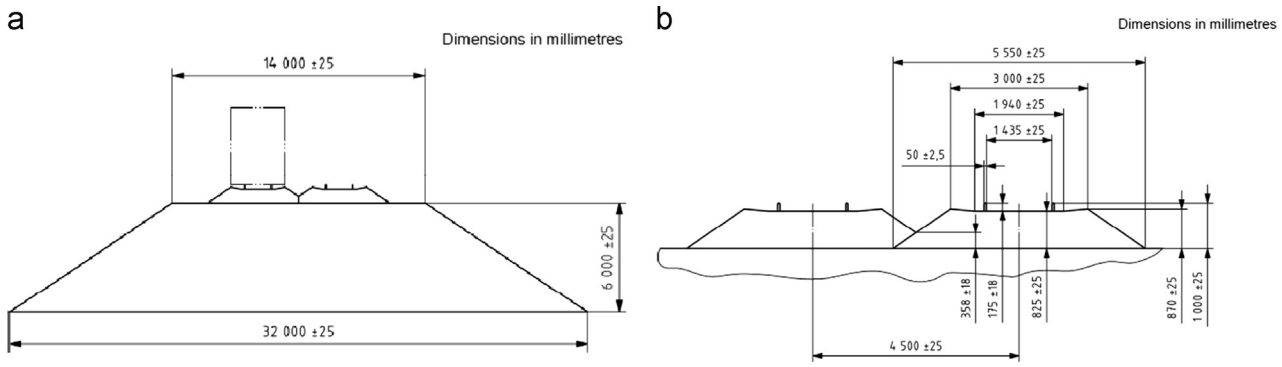

Fig. 2. Embankment (a) and double track ballast and rail (b) layout (TSI HS RST, 2008).

2.1. Description of the models

Wind tunnel tests were performed on a 1:45 ETR500 scale model with the standard embankment scenario which represents, as mentioned above, one of the two reference scenarios defined by the TSI standard (Fig. 2(a)). According to the European standard, a double track ballast and rail scenario was placed on top of the embankment (Fig. 2(b)).

The scale of the models was chosen to satisfy, for the smallest test section (DIA), the standard TSI requirement on the blockage ratio, a recommended maximum of 15%.

The train models were machined with a CNC milling machine from polyurethane modelling boards. The resulting model surface had very low roughness. The convoy is composed of the locomotive (live vehicle) and 1/2 of the first coach (dummy vehicle) to guarantee the correct boundary conditions, as required by the EN 14067-6. Two locomotive models were built: one to measure the overall forces and the other equipped with 96 pressure taps to measure the pressure field around the vehicle. The scenario was produced by machining polystyrene foam.

2.2. DIA test section

The first experimental campaign was carried out in the Politecnico di Milano DIA low turbulence wind tunnel. The test section was 1 m wide, 1.5 m high and 3 m long. The maximum wind velocity was 55 m/s and the turbulence intensity about 0.08%. The blockage ratio was 13% (wind angle 30°). The ratio between the length of the train model and the width of the tunnel (R_{t-wt}=0.77) was close to the limit suggested by CEN of 0.75. Wind flow was uniform (block profile) except for the presence of a small boundary layer on the test section floor. The boundary layer thickness $\delta_{99\%}$ (EN 14067-6, 2010) was measured and is compared with the embankment scenario height in Table 1.

To study how the length of the embankment influences the forces produced by the wind stream, measured on the train, during the experimental tests in the DIA wind tunnel four different scenario configurations were tested:

- Pseudo-infinite embankment (Fig. 3(a)), obtained by extending the scenario wall-to-wall (referred to below as WW). This configuration consisted of a fixed central part of the scenario, on which the power and trailer cars were placed. In order to manage wall-to-wall layout we had to replace the scenario parts in front of and behind the model for each wind angle investigated.
- Finite length embankment (referred to below as FL), consisting of an embankment located in the middle of the test section on which the train model was placed, plus 5 m (full scale) of embankment added in front, resulting in a free end (Fig. 3(b));

Table 1
Thickness of the floor boundary layer and turbulence intensity (Tu_x) in the different test sections.

Test section	$\delta_{99\%}$[mm]	$\delta_{99\%}/H_{emb}$ [-]	Tu_x [%]
DIA	40	0.3	0.08
CIRIVE	100	0.75	0.1
CIRIVE2	150	0.25	2

- To reduce flow distortion effects that could be caused by the finite length embankment solution, a 45° skewed nose was added upwind (Fig. 3(c), referred to below as N45);
- Finite length embankment plus 30° skewed nose added upwind (Fig. 3(d), referred to below as N30).
- Long finite length embankment with a 45° skewed nose added upwind (Fig. 3(e), referred to below as N45L). In this layout the length of the scenario in front of the train was 32 m (full scale), that is an increasing by a factor of 6 with respect to N45.

For all the configurations described, various wind angles were analyzed and are summarized in Table 2.

It is evident that for small angles it is not possible to use the wall-to-wall layout, since the length of the WW scenario increases as the wind angle decreases from 90° to 0°. At very low wind angles (0°, 10° and 20°) the scenario is bounded at the beginning of the test section and a small 45° skewed nose is added to the upwind side of the embankment. At 0° the length of the scenario in front of the train is 90 m full scale.

For yaw angles from 50° to 90°, the configurations with noses (N45, N30) were not tested because the closeness of the model to the wall of the test section creates problems with the end layout conditions.

The embankment scenario was placed directly on the floor of the wind tunnel.

2.3. CIRIVE1 test section

The second wind tunnel test section used was the low turbulence—high speed test section of the Politecnico di Milano wind tunnel (CIRIVE1). The section was 4 m wide, 4 m high and 6 m long. The maximum wind velocity was 55 m/s and the turbulence level about 0.1%. In these tests the blockage ratio was 4% (wind angle 30°). The ratio between the length of the train model and the width of the tunnel R_{t-wt} was 0.19, significantly lower than the CEN limit of 0.75. The distance from the upstream end of the ground model to the leading edge of the train model was 162.5 m full scale (see Table 4). The test section was equipped with a turntable to vary the wind angle. In the experimental tests at CIRIVE wind tunnel only the pseudo-infinite embankment configuration was investigated (Fig. 3(f), referred to below as WW2). The wind angles shown in Table 2 were tested. In this test section too,

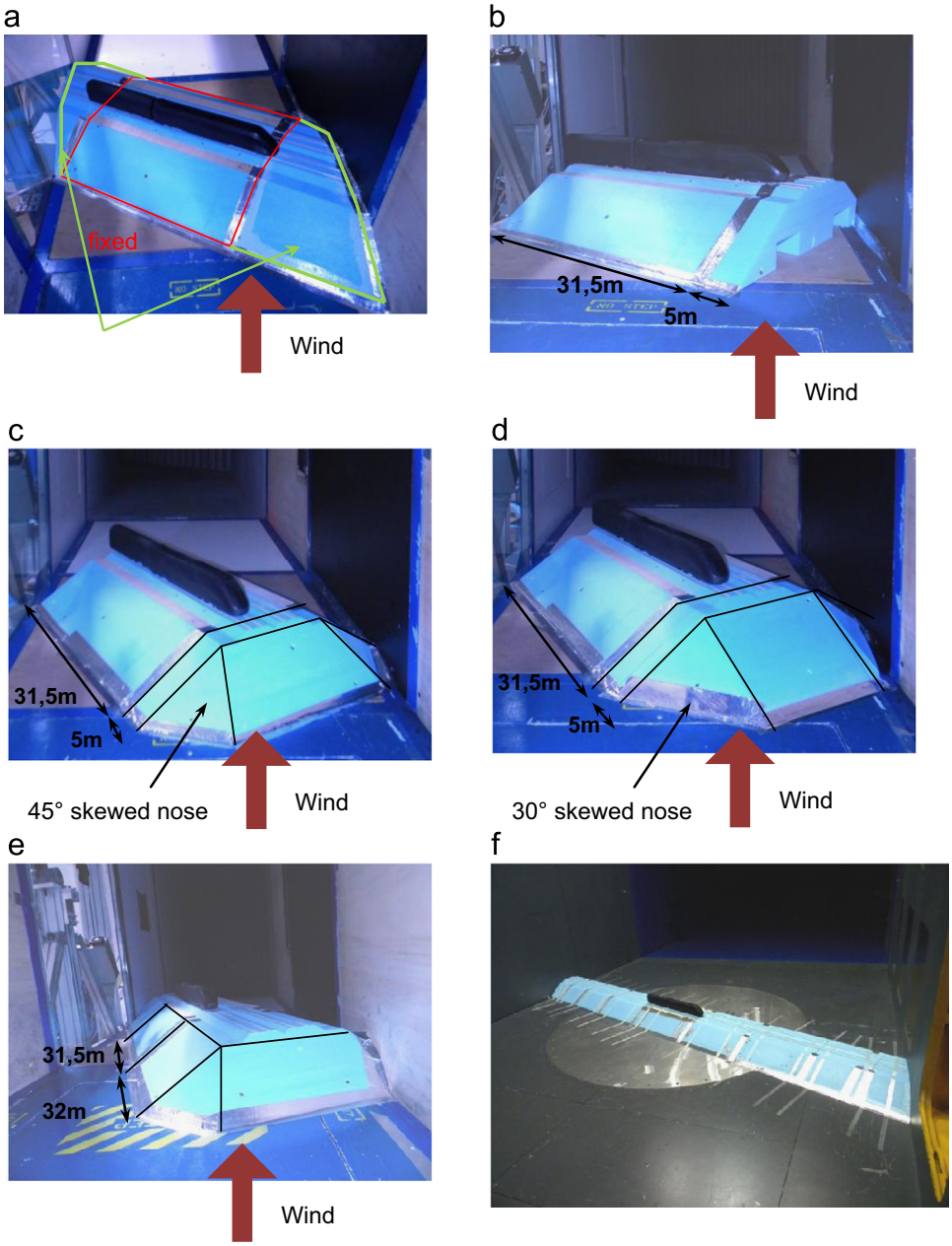

Fig. 3. DIA test section: wall-to-wall layout WW (a), FL layout (b), N45 layout (c), N30 layout (d), N45L layout (e). CIRIVE1 low turbulence test section, wall-to-wall layout WW2 (f). All dimensions are full scale values.

Table 2
Wind angle ranges tested at DIA and CIRIVE1 wind tunnels.

Wind tunnel	**DIA**					**CIRIVE1**
Config.	**WW**	**FL**	**N45**	**N30**	**N45L**	**WW2**
Angles	From 0 to 90° in steps of 10°	From 10 to 70° in steps of 10° and 90°	10, 20, 30 and 40°	10, 20, 30 and 40°	10 and 20°	30, 40, 50, 70 and 90°

the embankment scenario was placed directly on the floor of the wind tunnel. The flow had a vertical block mean wind speed with a wall boundary layer height of 100 mm (Table 1).

2.4. Measurement systems

For both the experimental campaigns described in this paper, DIA and CIRIVE1, the same models and measurement systems were adopted.

The model was designed to house a 6-component force balance (ATI mini45) to measure the aerodynamic force. The balance mounting side was linked to two plates: the upper one was rigidly linked to an aluminium chassis set inside the vehicle model while the lower one is connected to the ground by means of two beam elements. The full scale ranges for each component of the balance are reported in Table 3. The maximum error on M_x (rolling moment coefficient) and F_y (lateral force) are respectively 0.10% and 0.50% of the full scale load.

The reference system adopted for the definition of the aerodynamic forces was fixed to the car body and its origin coincides with the centre between the bogies, as specified by the standard EN 14067-1 (2003) (Fig. 4). X is the longitudinal axis, in the direction of movement, Z is the vertical axis, directed downwards, and Y is perpendicular to define a right-handed coordinate system. Force and moment coefficients are expressed in a non-dimensional form as in the standard EN 14067-1 (2003):

$$C_{F_i} = \frac{F_i}{(1/2)\rho A U^2} \quad C_{M_i} = \frac{M_i}{(1/2)\rho A h U^2} \quad i = x, y, z \tag{1}$$

where U is the wind speed, $F_i(i=x,y,z)$ are the aerodynamic force components in the train's reference system and M_i are the corresponding moments, evaluated in correspondence with the point P on the centre line of the top of the rail (Fig. 4). In Eq. (1), ρ is the air density, h is 3 m, and A is a standard reference surface of 10 m^2. Wind angles are considered positive when train is located on the upwind rail. The lee rail rolling moment coefficient is also evaluated $C_{Mx,lee}$ (EN 14067-1, 2003).

The power car train model was instrumented for pressure measurements: 96 taps were positioned on the model surface, especially on the nose and on the surfaces connecting the side to the upper part of the car body, where higher pressure gradients occur. Fig. 5 shows the layout of the pressure taps for some of the instrumented sections.

The surface pressure measurements were made using high-resolution multi-channel pressure scanners (PSI Initium with ESP-DTC pressure scanners, range ± 7 kPa, accuracy $\pm 0.10\%$ FS), located outside the model. PVC tubes were used to connect the pressure taps to the scanner. Wind speed was measured by a pitot tube, connected to low-pressure micro-manometers. The pitot tube was placed upstream of the model, at the height of the vehicle's geometric centre, in undisturbed flow. For all the tests, a sampling frequency of 200 Hz and a time window of 60 s were adopted.

Table 3
Characteristics of the dynamometric balance ATI mini45.

$\pm F_x$ [N]	$\pm F_y$ [N]	$\pm F_z$ [N]	$\pm M_x$ [N m]	$\pm M_y$ [N m]	$\pm M_z$ [N m]
145	145	290	5	5	5

3. Wind tunnel tests: Results

The wind tunnel experimental campaigns had three final aims. First, to analyse the Reynolds number effect on the force and pressure coefficients. Second, to study the effect on flow of different reproductions of the embankment scenario (wall-to-wall, finite length with and without nose, etc.). Third, to understand if the aerodynamic coefficients were sensitive to the distance between the wind tunnel walls and ends of the vehicle model (wall proximity effects).

The first two results will be obtained by analysing the data sets collected during the first experimental campaign in the DIA wind tunnel.

As concerns the third aim, it is important to point out that in the TSI standard, which requires tests with the embankment scenario, there are no indications for train model length, embankment model length and wind tunnel width. On the other hand, in the standard EN 14067-6, for the Single Track Ballast and Rail scenario, two requirements are introduced:

- the distance from the upstream end of the infrastructure model to the leading end of the train model (below referred to as L_{up}, see Fig. 4) must be at least 8 m (in full-scale dimensions);
- the ratio of the total length of the train model to the width of the tunnel (below referred to as R_{t-wt}) should not be less than 0.75.

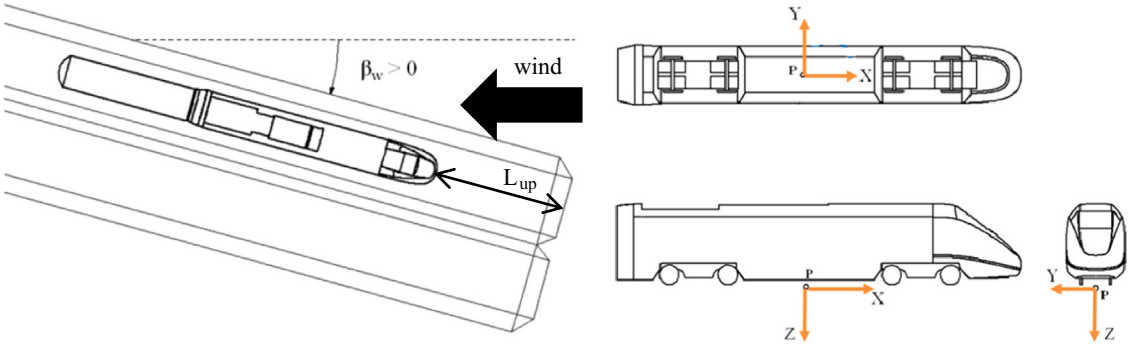

Fig. 4. Positive wind angle and train reference system.

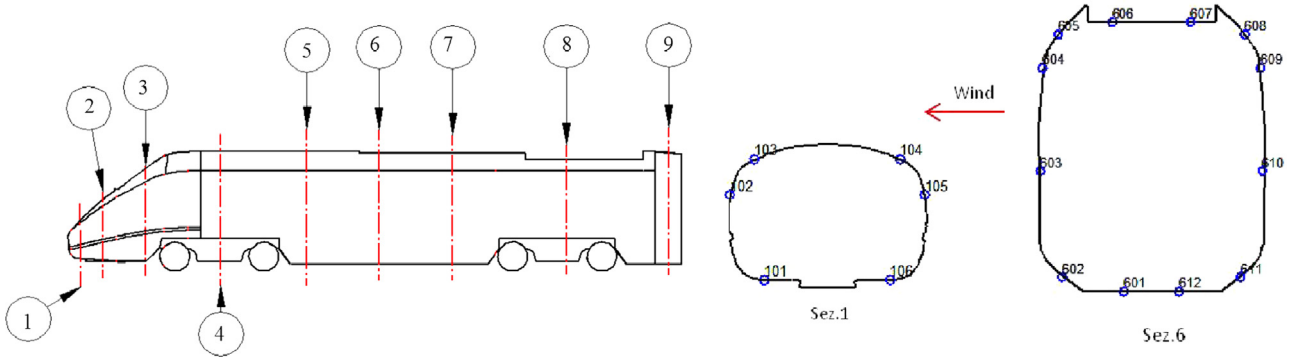

Fig. 5. Pressure taps layout.

Table 4
Blockage factor x_B, upwind embankment length L_{up}, ratio vehicle length to wind tunnel width R_{t-wt}: WW2 (wall-to-wall at CIRIVE1), WW (wall-to-wall at DIA) and FL2 (finite length at CIRIVE2).

Test	x_B (30°) [%]	L_{up} (30°) [m]	R_{t-wt} [-]
WW2	4	162.5	0.19
WW	13	27.5	0.77
FL2	12	54	0.25

To evaluate the wall proximity effects, the coefficients measured in the three different experimental campaigns were compared. In particular, the following configurations were considered:

- the reference scenario configuration tested in the DIA wind tunnel: the wall-to-wall arrangement (WW);
- the wall-to-wall configuration tested in CIRIVE1 (WW2);
- the finite length configuration tested in CIRIVE2 (Cheli et al., 2010) (FL2).[1]

Table 4 shows for these three configurations a number of parameters needed for the comparison, according to the requirements of the standard EN 14067-6: the blockage ratio x_B, the upwind embankment length L_{up} and the ratio of vehicle length to wind tunnel width R_{t-wt}.

According to the EN 14067-6, for blockage ratios between 5% and 15% corrections are needed. The coefficients calculated from measurements made at the DIA wind tunnel were corrected using a blockage correction method based on the dynamic pressure included in EN 14067-6, according to the following formula:

$$\frac{C_{Ff}}{C_F}=\frac{q_\infty}{q_M} \tag{2}$$

where the subscript f stands for "corrected value", q_∞ is the dynamic pressure of the undisturbed flow and q_M is the dynamic pressure measured above the model.

For the comparison between different experimental campaigns (DIA, CIRIVE1 and CIRIVE2), the data cannot be corrected with this method since the dynamic pressure at the model location was not available for all the data sets. In these cases, all the coefficients (also those measured at DIA) are corrected with another less accurate but always applicable method, suggested by ESDU Item No. 80024 (1980) and based on the blockage-area-ratio:

$$\frac{C_{Ff}}{C_F}=\left(1-\frac{S_T}{A_{WT}}\right)^2 \tag{3}$$

In Eq. (3), A_{WT} is the cross-section area of the wind tunnel and S_T is the reference cross-section area of the body (train model+embankment).

In the next section the Reynolds effects will be shown in terms of force and pressure coefficients; then, a comparison between the coefficients measured with the different embankment layouts tested at the DIA wind tunnel will be presented only for the higher Reynolds number. Finally, a comparison between the different experimental campaigns is described only for the force coefficients, considering the same *Re* number.

[1] Tests with this configuration have been carried out with a 45° skewed nose only for yaw angles ranged in 0°–20°. The measurement system was different from that used in the DIA and CIRIVE1 tests: the aerodynamic forces were measured by an external dynamometric balance (196-6I Ruag), set inside the embankment scenario (for more detail, see Cheli et al., 2010).

3.1. Reynolds effects

In order to study the effects of the Reynolds number, only the reference wall-to-wall scenario layout (DIA wind tunnel section) is considered and the most important coefficients, concerning the effects of the cross wind and the risk of roll-over, are analysed: the rolling moment (Fig. 6(a)) and the vertical force aerodynamic coefficients (Fig. 6(b)). The lateral force coefficient is as important as the rolling moment coefficient but, since they have a very similar trend, only the latter one is shown.

In Fig. 6 the coefficients are shown as a function of the wind angle for seven different increasing Reynolds numbers up to $Re_{max}=2.2\times10^5$.[2] Considering the rolling moment coefficient (Fig. 6(a)), it is possible to divide the diagram into three angular sectors on the basis of the coefficient trend: an increasing trend, up to a maximum value recorded at 40°, a central sector with a negative slope, for angles of attack from 50° to 60° and then a constant trend. This trend has been found in the past by a number of researchers and is typical of all the leading vehicles of a convoy also in different scenarios (flat ground, single track ballast and rail, double track ballast and rail) (Cheli et al., 2010; Baker, 1991, 2002; Baker et al., 2004; Bocciolone et al., 2008). The angle where the coefficient reaches its maximum has been defined as the "critical angle" and is related to the transition from slender to bluff body behaviour. Fig. 6(a) shows that in the slender body behaviour sector the force coefficients are almost independent of the Reynolds number, as found for the embankment also by Schober et al. (2010). In the central sector, a larger scatter appears but it is due also to the high dependence of coefficients in this zone on the test layout conditions (as it will be shown in the next sections). Finally, in the constant trend sector, a low dependence on the Reynolds number can be observed: in particular, as the Reynolds number increases, the rolling moment coefficient decreases slightly.

It is possible to draw conclusions similar to those in paper (Cheli et al., 2011d). In this paper the Reynolds number effects on the same vehicle (ETR500 train) were investigated in depth with wind tunnel tests using a simplified infrastructure scenario reproducing only a standardised single track with ballast and rail (STBR).

The trend of the vertical force coefficient (Fig. 6(b)) is similar to that of the rolling moment: also for this component, the maximum absolute value is in correspondence of $\beta_w=40°$. From the analysis of Fig. 6(b) it is possible to see that the vertical force coefficient shows a dependence on Reynolds number a little higher than that found for the rolling moment coefficient, especially for angles of attack ranged in between 30° and 60°. Moreover, for this component, the coefficient increases increasing the *Re* number (of about 15% in the range [30°–60°]). The same behaviour has been found for the same train on Single Track Ballast and Rail (Cheli et al., 2011d). The comparisons with the paper Cheli et al. (2011d) suggest the Reynolds effect is mainly influenced by the vehicle aerodynamics than by the scenario.

Fig. 7 shows the surface pressure coefficients on two different train sections as a function of the Reynolds number: section 1 is in the front part and section 6 is in the middle between the bogies (see Fig. 5). Two wind angles, 30° and 90°, are investigated. It can also be seen from the pressure data that the Reynolds number effects are quite small. In particular, the central body of the vehicle is almost independent of the Reynolds number (Fig. 7(b) and (d)); section 1, in correspondence with the nose, seems to be slightly more sensitive in the underbody (Fig. 7(a)) and in the windward upper part (Fig. 7(c)). Accordingly, in

[2] The maximum Reynolds number could not be reached at high wind angles since the increase of the blockage reduced the facility's performance.

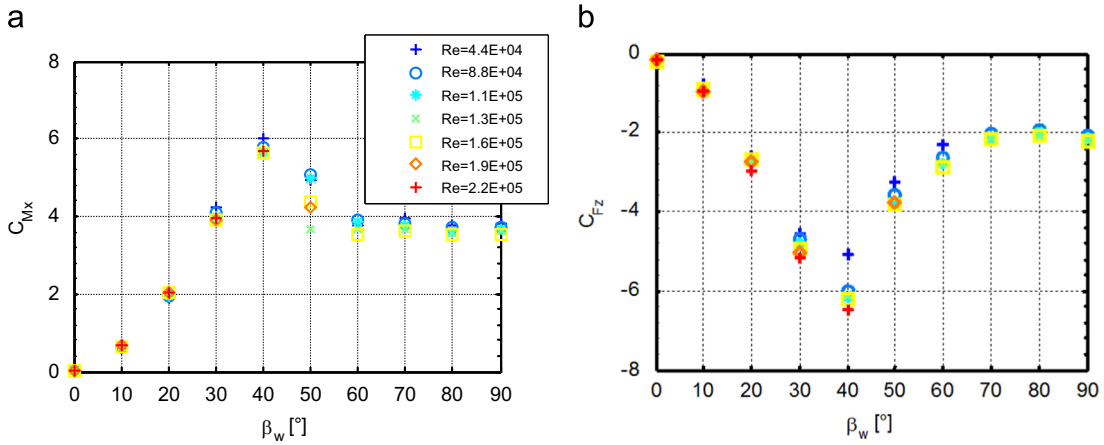

Fig. 6. DIA wind tunnel, wall-to-wall scenario: rolling moment (a) and vertical force (b) aerodynamic coefficients at different Reynolds numbers.

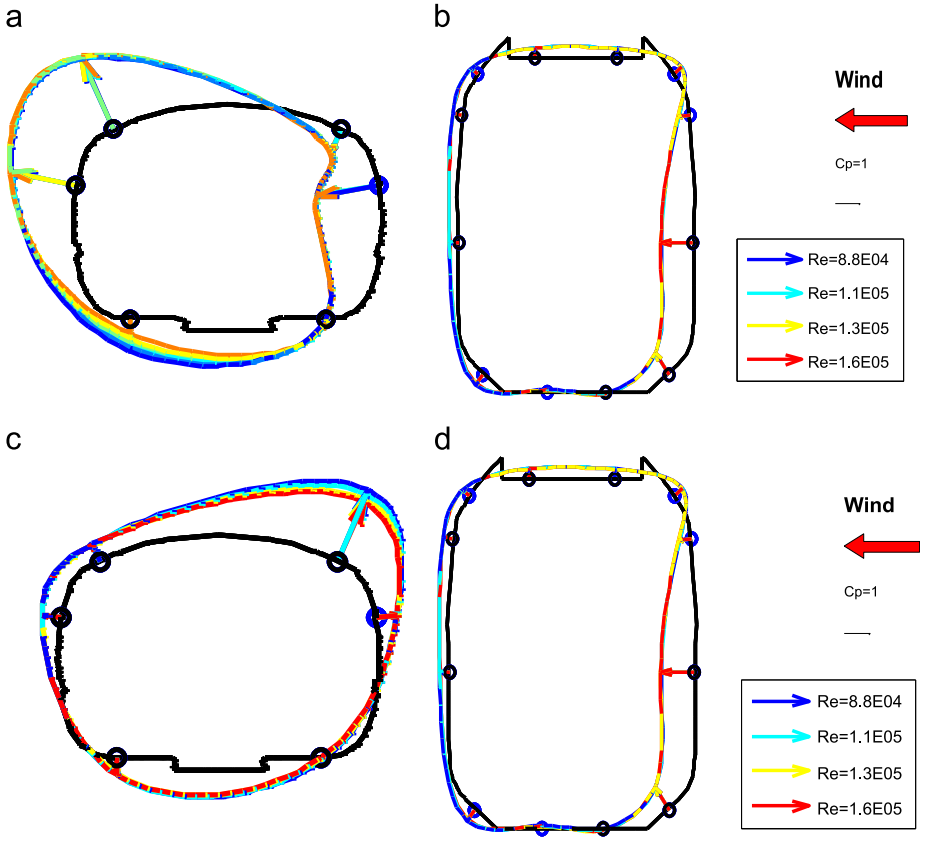

Fig. 7. DIA wind tunnel, wall-to-wall scenario, surface pressure coefficients at different Reynolds numbers: (a) wind angle 30°—section 1, (b) wind angle 30°—section 6, (c) wind angle 90°—section 1 and (d) wind angle 90°—section 6.

Cheli et al. (2011d), it was found that the area most sensitive to the Reynolds number was that in the windward upper part: as a consequence, also from this comparison it is possible to conclude that ground scenarios do not modify significantly the Reynolds number dependence of a train geometry.

3.2. *Effects of infrastructure modelling*

Since there is no significant sensitivity to the Reynolds number in the force coefficients, the comparisons between the different embankment setups will be shown for only one Reynolds number value ($Re = 1.6 \times 10^5$).[3]

Fig. 8 shows the three force and moment aerodynamic coefficients as a function of the wind angle for five different embankment scenario end layouts:

[3] $Re = 1.6 \times 10^5$ represents the greatest number for that all yaw angles have been tested.

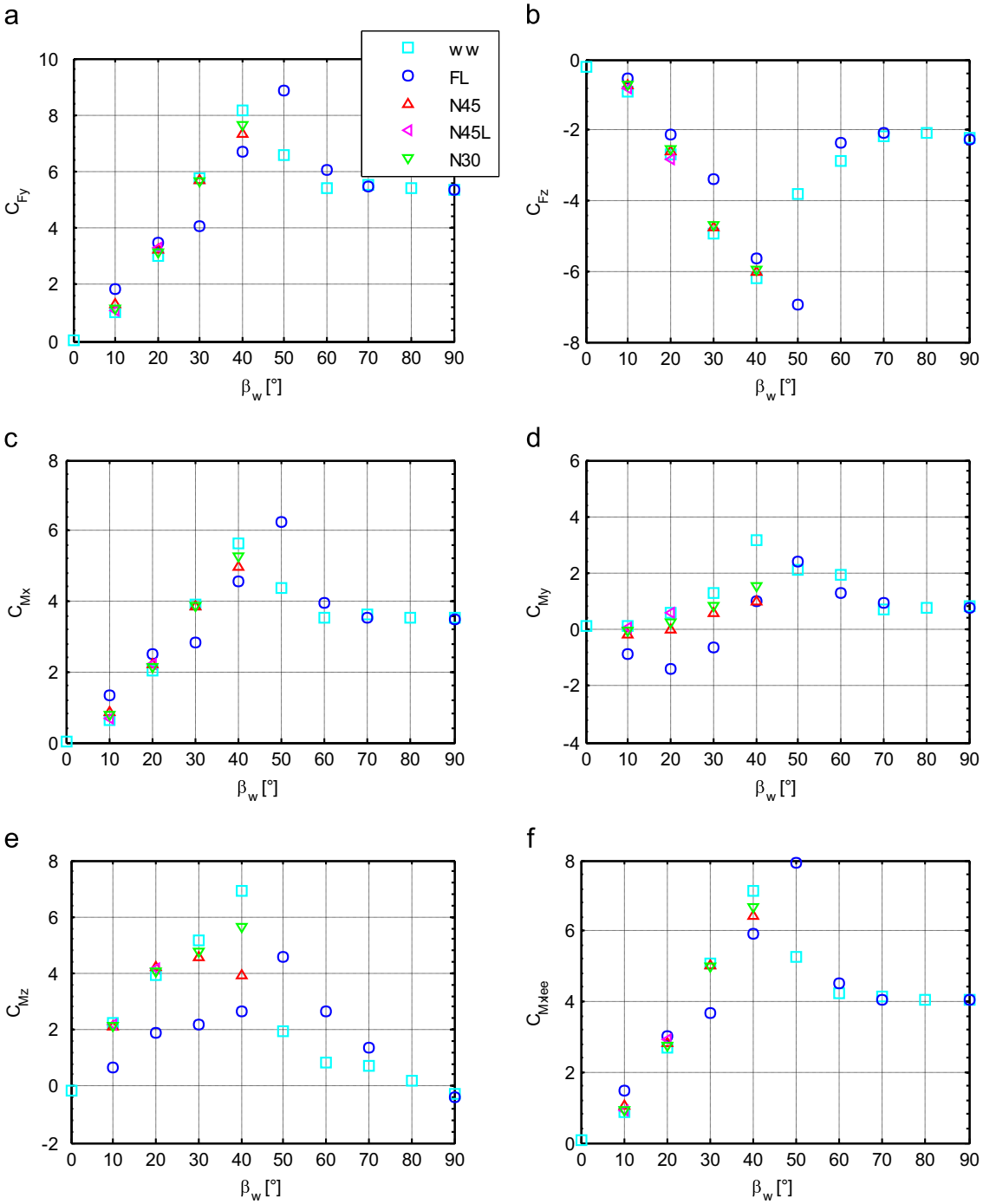

Fig. 8. DIA wind tunnel, Reynolds number 1.6×10^5, force and moment coefficients for different end layouts: C_{Fy} (a), C_{Fz} (b), C_{Mx} (c), C_{My} (d), C_{Mz} (e) and $C_{Mx,\ lee}$ (f).

- wall-to-wall (WW);
- finite length (FL);
- upwind nose with 45° slope (N45);
- upwind nose with 30° slope (N30);
- upwind nose with 45° slope and long front part scenario (N45L).

Generally, it is assumed that the most realistic situation is the wall-to-wall layout since the scenario is extended up to the wind tunnel walls and the flow deviations due to the scenario end conditions are significantly reduced.

Looking at the lateral force and rolling moment coefficients (Fig. 8(a) and (c)), the most important in rollover risk evaluation, it can be seen that, at low wind angles, there is a good match between the results in the WW layout and in the nose layouts (N45, N30 and N45L). FL layout data shows a similar trend, but the values differ significantly from the WW data. On the other hand, at high angles of attack, where the effects of embankment ends are less significant, the FL coefficients are very close to the WW values.

The vertical force coefficient (Fig. 8(b)) appears even less sensitive to the end conditions than the lateral force coefficient, but the FL values still differ from that of the other layout, in particular at 30°.

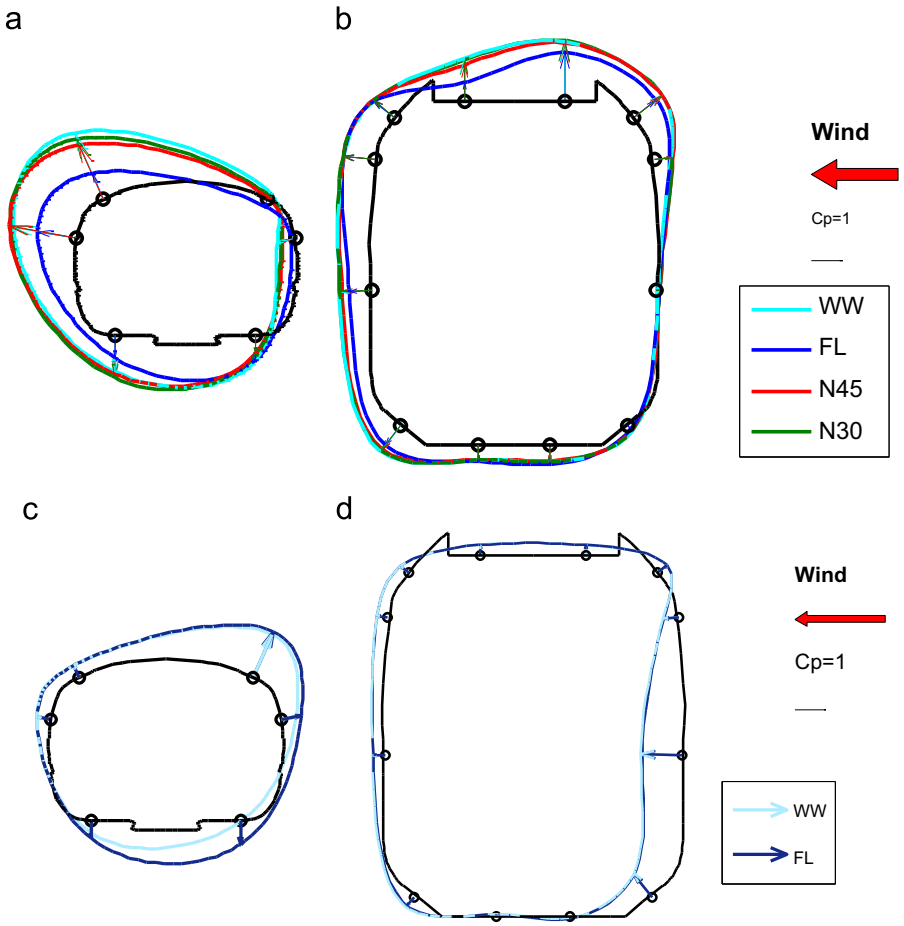

Fig. 9. DIA wind tunnel, Reynolds number 1.6×10^5, pressure coefficients for different end layouts: section 1, $\beta_w = 30^\circ$ (a) and section 6, $\beta_w = 30^\circ$ (b), section 1, $\beta_w = 90^\circ$ (c), section 6, $\beta_w = 90^\circ$ (d).

The aerodynamic yawing moment (Fig. 8(e)) shows a good match of the data, excluding the FL layout, for wind angles up to 30°. The aerodynamic pitching moment (Fig. 8(d)), which has very low values and is mainly associated with the longitudinal force coefficient, shows a certain scatter also at low yaw angles.

Considering all the force coefficients, it can be concluded that, with the exception of the finite length layout (FL), the other end conditions are generally in good agreement with the reference wall-to-wall data. Moreover, if the lateral force and the rolling moment are analysed, the lower N30 nose slope is better (the coefficients are nearer to the reference ones of the wall-to-wall configuration) than the N45 and the scenario with a longer upwind part (N45L) gives more accurate results than a shorter one (N45).

Nevertheless, close to the critical angle data dispersion increases: we have already pointed this out in the Reynolds number effects section and, again, we can say that around this angle the train aerodynamic is very sensitive to the test layout conditions (that are the geometry of the infrastructure but also, as it will be shown in the next section, the distance from the wind tunnel walls) so that discrepancies in the results are more likely.

Fig. 9 shows the surface pressure distribution measured with different end layouts on the two section 1 and 6 for the two yaw angles 30° and 90°. It is clear that, at the lowest wind angle (Fig. 9(a) and (b)), the surface pattern in FL completely differs from the others, confirming that this set-up, with a very short upwind embankment length (only 5 m, at real scale), is not suited for reliable results in the range where the vehicle behaves as a slender body. In particular, from the analysis of the pressure pattern it is possible to conclude that the differences found in the force coefficients are mainly due to pressure variations especially in the underbody zone and in the upper part of the vehicle.

On the other hand, at $\beta_w = 90^\circ$ (Fig. 9(c) and (d)), the pressure distributions evaluated with the two configurations WW and FL are very similar, except for the under-body zone of the nose.

In section 6 (Fig. 9(b)), the N45 and N30 layouts data match the WW reference data very well (even if, also in this case, the upwind embankment length is only 5 m, at real scale) while in Section 1 there are some differences, in particular in the leeward upper part, where the maximum suction value slightly changes in the different layouts. This confirms the previous statement that the model front part is the most sensitive to the end conditions.

3.3. *Wall proximity effects*

As described in the previous section, to evaluate the wall proximity effects, force balance tests were performed on the same train model but in a large test section (CIRIVE1), where blockage effects were negligible: the embankment scenario was extended wall-to-wall with a very long part in front of the vehicle model (L_{up} higher than 150 m full scale, see Table 4) and the ratio between vehicle length and wind tunnel width was very low ($R_{v,wt}$ lower than 0.2, see Table 4). In Fig. 10 these results, referred to as WW2, are compared to those with the same end layout (wall-to-wall) in the DIA wind tunnel, referred to as WW. In addition, the same figure also shows data from previous tests on a 1/10 model (CIRIVE2, Cheli et al., 2010). These data series are referred to as FL2. It is important to point out that WW has a very high value for

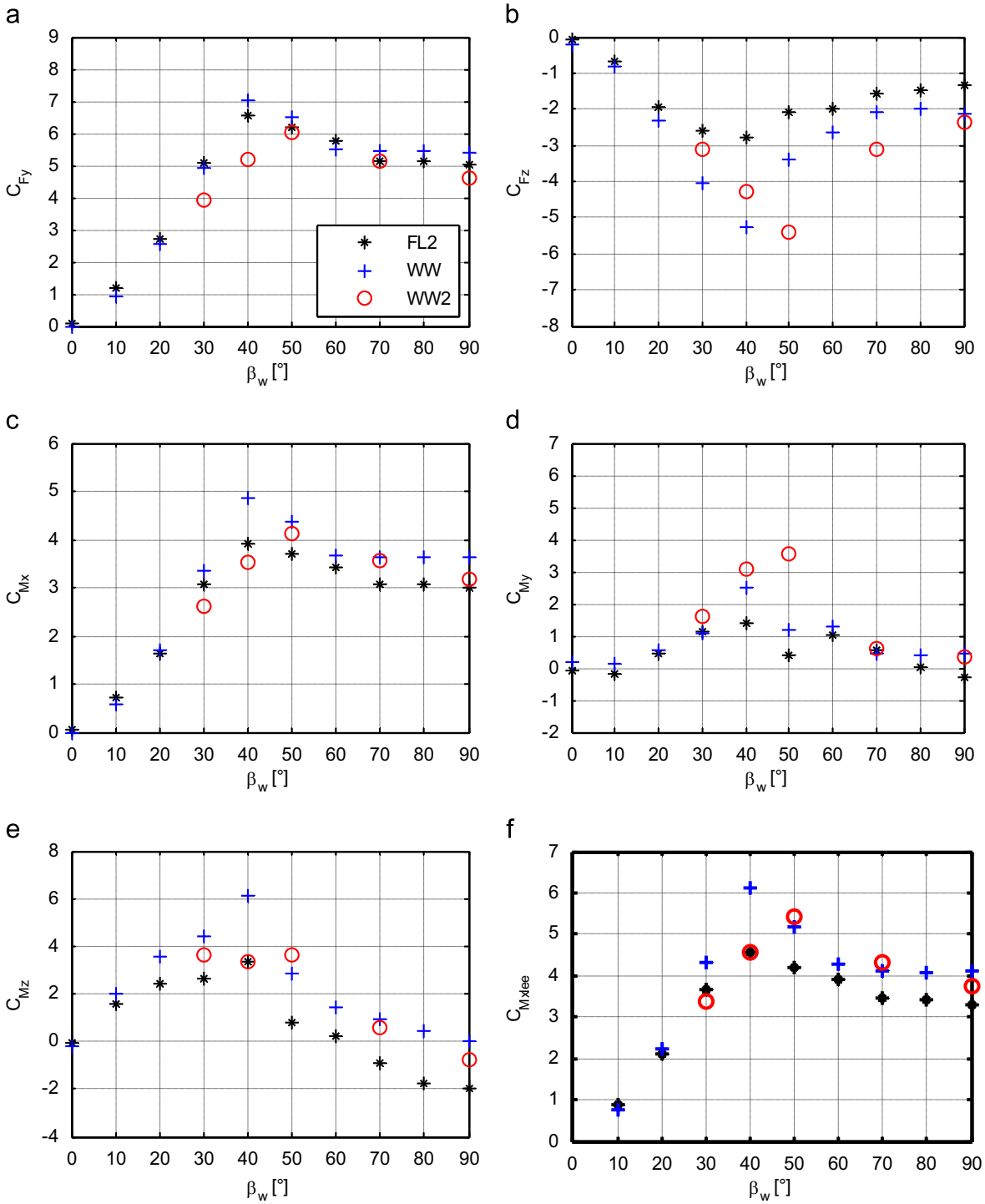

Fig. 10. Force and moment coefficients for different wind tunnel test set-up, corrected for the blockage effect ($Re = 1.1 \times 10^5$): C_{Fy} (a), C_{Fz} (b), C_{Mx} (c), C_{My} (d), C_{Mz} (e) and $C_{Mx,lee}$ (f).

R_{v-wt} (see Table 4), meaning that, in this configuration, the vehicle model ends are very close to the wind tunnel walls; on the other hand, WW2 and FL2 have similar R_{v-wt} ratios (see Table 4). The WW2 set-up, with a blockage factor lower than 5% and a very long upwind embankment part L_{up} (longer than 150 m, Table 4) is the most similar to real conditions where upwind embankment length tends to infinite values.

As mentioned above, to compare the results obtained with the three wind tunnel set-ups all coefficients were corrected to take into account the blockage factor according to the formula in Eq. (3).

First, a comparison between the two set-up configurations WW and FL2 is made. Then, the data obtained in the CIRIVE1 section (WW2) are compared with the other two data series and the differences are discussed.

3.3.1. *Comparison between WW and FL2*

Looking at the lateral force coefficient (Fig. 10(a)), it can be seen that there is a very good match between the FL2 configuration (CEN reference data) and the WW wind tunnel set-up at all wind angles. The maximum percentage error, in the range of significant

yaw angles (20°–70°) is lower than 7% while the mean error in the range is about 5%. Good agreement on the lateral force component between these two configurations is obtained in spite of the different model scales and infrastructure set-ups (1:10 with finite length scenario for the FL2 vs 1:45 with wall-to-wall scenario for the WW). Moreover, as already underlined, the two configurations have very different values of the R_{v-wt} ratio, and, as a consequence, different wall proximity effects.

If the rolling moment coefficient is studied (Fig. 10(c)), it is found that the gap between the two data series, WW and FL2, is higher than that measured for the lateral force, although the mean error is lower than 12% also in this case. A number of studies in the literature (Cheli et al., 2010, 2011a, 2011b) have shown that the rolling moment is mainly associated with the contribution of the lateral force: in fact, not only the vertical force is generally lower in modulus than the lateral one but also its arm (distance from the rails center of the application point in lateral direction) is significantly lower. The lateral force is typically applied at a constant height as the wind angle varies. This means that the greater discrepancies found between the rolling moment coefficients must be ascribed to a difference in the application height of the lateral force, which can be linked to differing boundary layer profiles. In fact, looking at Table 1, the profile height divided by the embankment model height ($\delta_{99\%}/H_{\mathrm{emb}}$) is lower at the CIRIVE2 than at the DIA wind tunnel: this is in agreement with the values of rolling moment coefficients, which are lower with the FL2 configuration than with the WW set-up.

The match between these two wind tunnel set-ups is poorer when the vertical force coefficient is analysed (Fig. 10(b)): for this component too, the trend of the two data series is equivalent (critical angle at 40°) but the discrepancies in the absolute values are higher. The reason can be found by considering that the vertical force, directed upwards, is mainly associated with the pressure distribution in both the roof and the underbody zones. In this latter zone, the flow velocity and, as a consequence, the pressure, are strongly influenced by the amplitude of the gap between train and infrastructure and by the correct reproduction of the underbody shape. In this case, the very small scale of the model adopted for the tests in the DIA wind tunnel (WW configuration) is probably the cause of insufficient accuracy in the construction of the model in the underbody zone.

The lee-rail rolling moment coefficient, which accounts for the combined effects of both the lateral and the vertical force, is penalised by the disagreement found for the vertical force. The trend of two data series is similar, but the differences become significant for wind angles of 40° and 50°, that is around the critical angle, exactly where greater differences were found for the vertical force coefficient.

Finally, the agreement between FL2 and WW is good for C_{My} while, for C_{Mz} the coefficients measured with the WW are generally higher than those measured with FL2. Also in this case, the reason could be the different arm of the lateral force in the two wind tunnel set-ups.

In conclusion, from a comparative analysis between the FL2 and WW wind tunnel set-ups, it can be concluded that, if the vertical force is disregarded (considering that the discrepancies found can be ascribed to modelling problems), the agreement between the measured coefficients is good, even if the two configurations have very different values for the R_{v-wt} ratio: this means that wall proximity does not have a significant effect on the aerodynamic forces if the limit value of 0.75, prescribed by the standard CEN, is respected.

3.3.2. Analysis of WW2 data

Considering the coefficients measured in the CIRIVE1 section with the 1:45 scale model on the wall-to-wall embankment (WW2 series), it is possible to note that, for all the force and moment components shown in Fig. 10, the maximum absolute value is reached at a wind angle of 50° (which represents, as a result, the critical angle) while, with the first two set-ups analysed (CIRIVE2 and DIA), the critical angle was 40°. It is authors' opinion that this main discrepancy is associated with the different values of upwind embankment length simulated in the three configurations.

In fact, as already highlighted, the WW2 configuration has a very long upwind embankment part (L_{up}=162.5 m) with respect to that of the other two configurations (L_{up}=54 m for FL2 and L_{up}=27.5 m for WW): this means that, while in the FL2 and in the WW wind tunnel set-ups, the distance from the upstream end of the infrastructure model to the leading end of the train model is of the order of the vehicle length, in the CIRIVE1 section, the same distance is about three-five times greater. This very long embankment section leads to a different development of the flow in front and, as a consequence, on the rear of the train model: in particular, a long infrastructure section tends to align the flow along the vehicle and to move, at higher angles (from 40° to 50°) the transition from slender to bluff body behaviour. As a consequence, the maximum value reached by all the coefficients with a greater upwind embankment length is higher and the shorter embankment (compliant with the TSI requirements) is not conservative.

In conclusion, the upwind embankment length proves to be a key parameter in determining the aerodynamic coefficient just around the critical angle, in the yaw angle transition range.

A further confirmation of this hypothesis comes from the numerical CFD study reported in Cheli et al. (2014). In that paper, the coefficients of the same ETR500 train on an embankment are numerically evaluated for two different domains: the first exactly reproduces the DIA wind tunnel set-up while the second simulates open field conditions, with an upwind embankment length of 190 m. Comparison between the two data series referred to the two domains shows that the differences arise just in the transition zone and the critical angle moves from 40°, with the first domain, to 50°, with the open field simulation. On the other hand, for angle up to 40°, the coefficients evaluated with the two domains are very similar (Cheli et al., 2014).

Looking at the lateral force coefficient (Fig. 10(a)) and at the rolling moment coefficient (Fig. 10(c)), it can be seen that the coefficients measured in the CIRIVE1 wind tunnel (red circles, WW2) are different (lower) than those evaluated with the same model of train and infrastructure in the DIA wind tunnel, at low yaw angles too (30°–40°), when the model behaves as a slender body. The reason for this discrepancy is the different heights of the vertical wind speed profile simulated in the two wind tunnels: as shown in Table 1, the vertical profile height in the CIRIVE1 wind tunnel corresponds to 75% of the embankment model height, while in the DIA wind tunnel the profile height is about half. In fact, also from the comparison between the experimental WW2 series and the data calculated by the numerical simulation with open field conditions, it is possible to note that all the experimental coefficients are lower than the corresponding numerical ones although the trend is the same (Cheli et al., 2014).

Considering the comparison between the two layouts WW2 and WW (tested with the same vehicle model 1:45 scaled) in terms of vertical force coefficient (Fig. 10(b)), it is possible to observe that the maximum value reached in the two configurations is almost the same (about 5.5), significantly higher than the maximum measured in the FL2 layout (tested with a different model of the same train, 1:10 scaled). Also at 90° the two series show a similar value. On the other hand, as already underlined, the different upwind embankment lengths of the two configurations lead to a modification of the critical angle, where the coefficient reached its maximum value. Moreover, especially for this coefficient, the different embankment layouts modify the data not only around the critical angle but at almost all tested yaw angles, except the 90°.

The C_{my} and C_{mz} coefficients, calculated for the WW2 configuration, are similar that found for the WW layout, except for the angles around 40°–50°, where the effect of the different lengths of the upwind embankment part modified the flow around the vehicle, as described at the beginning of this section (Fig. 10(d) and (e)).

Finally, the lee-rail rolling moment coefficient (Fig. 10(f)) with WW2 is significantly lower than that measured with WW at 30° and 40° while, at higher wind angles, agreement between the two data series is very good. This behaviour is due to the combined effect of lateral and vertical force coefficients: at 30° and 40°, the WW2 coefficients are both lower than the corresponding WW coefficients while, at higher angles, the lateral and vertical force coefficients balance each other and, as a consequence, the agreement in terms of lee-rail rolling moment coefficient is improved.

In conclusion, the tests carried out in the CIRIVE1 wind tunnel made it possible to highlight the effects of the upwind embankment length, especially in the range of wind angles around the critical angle.

4. Conclusions

The aim of this study was to evaluate the effects of embankment modelling (scenario length, presence of the nose, etc.) on the determination of vehicle aerodynamic coefficients using wind tunnel tests on scale models. In particular, three aspects were analysed:

1. the Reynolds number effect on the force and pressure aerodynamic coefficients;
2. the effect of different end layouts with respect to the reference wall-to-wall configuration;
3. the influence of upwind embankment length (L_{up}) and wall proximity effects, monitored by the parameter R_{v-wt};

As far as the *first point* is concerned, it is found that, in the range of *Re* numbers simulated (up to 2.2×10^5), the *Re* number has no significant influence on the main force coefficients, at low and high wind angles. A small Reynolds effect has been observed at wind angles around the critical one, especially in the vertical force coefficient, which increases increasing the Reynolds number. Some variations in pressure distribution were observed mainly on the vehicle nose as the *Re* number varied, while its effect is negligible if the body is considered. Moreover, a comparison with literature data, measured on the same train but with a different scenario (STBR), has allowed to conclude that the Reynolds effects are mainly depending on the vehicle aerodynamics than on the infrastructure scenario.

To investigate the *second point*, experimental tests were performed with different embankment end layouts (wall-to-wall, finite length with and without noses, etc.) on a 1:45 scale ETR500 train model in the DIA wind tunnel section (1.5×1 m wide). From the coefficients measured it is possible to conclude that, in the 10°–40° range of wind angles, all the data series, except for those measured with the finite length layout (FL), are generally in good agreement with the reference wall-to-wall data (error range $\pm 10\%$). Moreover, if the lateral force and the rolling moment are analysed, the lower N30 nose slope is better (the coefficients are nearer to the reference ones of the wall-to-wall configuration) than the N45 and the scenario with a longer upwind part (N45L) gives more accurate results than a shorter one (N45).

The greater differences were found in correspondence with the critical angle: around this angle the train aerodynamic is very sensitive to the boundary conditions so that discrepancies in the results are more probable.

A new experimental campaign with the same vehicle and infrastructure models was then carried out in the wider wind tunnel section CIRIVE1 (4×4 m wide) with the wall-to-wall configuration, to analyse the effect of upwind embankment length and wall proximity *(third point)*. In addition, the aerodynamic coefficients measured with the two wind tunnel set-ups were compared with the reference data for the ETR500 train given in the standard EN 14067-6, obtained in a previous experimental campaign carried out in the CIRIVE2 test section (14×4 m wide) on a 1:10 scale model with a finite length embankment with nose. The CIRIVE1 set-up is the closest to real conditions because it has a very low R_{v-wt} ratio and a very high upstream embankment length (L_{up}=162.5 m and R_{v-wt}=0.19), while the other two set-ups have similar blockage factors and significantly shorter upwind embankment lengths ($L_{up} < 55$ m). In any case, the CIRIVE2 has an R_{v-wt} value (0.25) significantly lower than that of DIA (R_{v-wt}=0.77).

The comparison between the CEN data (FL2) and the DIA data (WW) allowed us to conclude that agreement between the coefficients measured was good (apart from the vertical force coefficient), even if the two configurations had very different values for the R_{v-wt} ratio: this means that wall proximity does not have a significant effect on the aerodynamic forces if the limit value of 0.75, prescribed by the standard CEN, is respected.

Comparison between the three data series showed that a significant variation in the upwind embankment length L_{up} leads to a modification of the critical angle, which moves from 40°, for low values of L_{up}, to 50°, in correspondence with L_{up}=162.5 m. The same behaviour was found in a CFD numerical study which had similar aims (Cheli et al., 2014). From all these results it is possible to conclude that upwind embankment length is a key parameter in determining the aerodynamic coefficients with the embankment scenario, because it can modify the angle where the transition from slender to bluff body behaviour occurs. The minimum value set for this parameter in the standard EN 14067-6 for the Single Track Ballast and Rail scenario (8 m) cannot be considered adequate for the embankment infrastructure.

Finally, it is important to underline that all the tests were conducted on static models and, as a consequence, they involve a certain degree of approximation in the results because they do not correctly simulate the relative velocity between wind and train and between wind and infrastructure. As reported in the introduction, previous numerical studies showed that this effect can be quantified in about 10% on the lateral force and rolling moment coefficients, for angles up to 30°.

In conclusion, static tests with the embankment scenario do not correctly reproduce the aerodynamic behaviour of a train running on an embankment and, moreover, depend on a number of set-up parameters which have to be well defined. Currently, the TSI standard requirements for wind tunnel tests with the embankment are not complete, because nothing is specified in terms of, for example, modelling configuration (i.e. wall-to-wall, finite length with or without nose), ratio between vehicle model and wind tunnel width (R_{v-wt}) or upwind embankment length (L_{up}). It is authors' opinion that a revision of the TSI standard on this matter is needed, either specifying a common, well-defined procedure for carrying out these tests or abandoning the embankment scenario in favour of more simple infrastructures (flat ground, Single Track Ballast and Rail, Double Track Ballast and Rail).

References

Baker, C.J., 1985. The determination of topographical exposure factors for railway embankments. J. Wind Eng. Ind. Aerodyn. 21 (1), 89–99 (1985).

Baker, C.J., 1991. Ground vehicles in high cross winds part1 steady aerodynamic forces. J. Wind Eng. Ind. Aerodyn. 5, 69–90.
Baker, C.J., 2002. The wind tunnel determination of cross wind forces and moments on a high speed train. Numerical Fluid Mechanics. 79. Springer-Verlag, Berlin, pp. 46–60.
Baker, C.J., Jones, J., Lopez-Calleja, F., Munday, J., 2004. Measurements of the cross wind forces on trains. J. Wind Eng. Ind. Aerodyn. 92, 547–563.
Baker, C.J., Cheli, F., Orellano, A., Paradot, N., Proppe, C., Rocchi, D., 2009. Cross-wind effects on road and rail vehicles. Veh. Syst. Dyn. 47 (8), 983–1022.
Baker, C.J., 2010b. The simulation of unsteady aerodynamic cross wind forces on trains. J. Wind Eng. Ind. Aerodyn. 98 (2010), 88–99.
Bocciolone, M., Cheli, F., Corradi, R., Muggiasca, S., Tomasini, G., 2008. Cross wind action on rail vehicles: wind tunnel experimental analyses. J. Wind Eng. Ind. Aerodyn. 96, 584–610.
Carrarini, A., 2007. Reliability based analysis of the crosswind stability of railway vehicles. J. Wind Eng. Ind. Aerodyn. 95 (7), 493–509.
Catanzaro C., Cheli, F. Rocchi, D. Schito, P. Tomasini, G., 2010. High-speed Train Crosswind Analysis: CFD Study and Validation with Wind-Tunnel Tests, Aerodynamics of Heavy Vehicles III: Trucks, Buses and Trains, Potsdam (D), September 2010.
Cheli, F., Corradi, R., Diana, G., Tomasini, G., 2004. A numerical-experimental approach to evaluate the aerodynamic effects on rail vehicle dynamics. Veh. Syst. Dyn. 41 (Suppl.), 707–716.
Cheli, F., Corradi, R., Rocchi, D., Tomasini, G., Maestrini, E., 2010. Wind tunnel tests on train scale models to investigate the effect of infrastructure scenario. J. Wind Eng. Ind. Aerodyn. 98, 353–362.
Cheli, F., Ripamonti, F., Sabbioni, E., Tomasini, G., 2011a. Wind tunnel tests on heavy road vehicles: cross wind induced loads—Part 2. J. Wind Eng. Ind. Aerodyn. 99, 1011–1024.
Cheli, F., Corradi, R., Sabbioni, E., Tomasini, G., 2011b. Wind tunnel tests on heavy road vehicles: cross wind induced loads—Part 1. J. Wind Eng. Ind. Aerodyn. 99, 1000–1010.
Cheli, F, Rocchi, D, Schito, P, Tomasini, G. 2011c. Steady and moving high-speed train crosswind simulations. In: Comparison with Wind-tunnel Tests, Ninth World Congress on Railway Research (WCRR 2011). 22–26 May 2011, Lille, France.
Cheli F., Rocchi D., Tomasini G., 2011d. Study of the Reynolds effects on aerodynamic coefficients of a railway vehicle through wind tunnel tests. In: 13th ICWE International Conference on Wind Engineering. , July 10–15, Amsterdam, The Netherlands.
Cheli, F., Corradi, R., Tomasini, G., 2012. Crosswind action on rail vehicles: a methodology for the estimation of the characteristic wind curves. J. Wind Eng. Ind. Aerodyn. 104–106, 248–255, http://dx.doi.org/10.1016/j.jweia.2012.04.006.
Cheli, F., Schito, P., Tomasini, G., 2014. Numerical investigation of the effects of embankment scenario on railway vehicle aerodynamic coefficients. J. Wind Eng. Ind. Aerodyn. (submitted for publication).
Diedrichs, B., 2003. On computational fluid dynamics modeling of crosswind effects for high-speed rolling stock. Proc. Inst. Mech. Eng. Part F J. Rail Rapid Transit 217 (F3), 203–226.
Diedrichs, B., Sima, M., Orellano, A., Tengstrand, H., 2007. Crosswind stability of a high-speed train on a high embankment. Proc. Inst. Mech. Eng. Part F J. Rail Rapid Transit 221 (F2), 205–225.
Ding, Y., Sterling, M., Baker, C.J., 2008. An alternative approach to modelling train stability in high cross winds. Proc. Inst. Mech. Eng. Part F J. Rail Rapid Transit 222 (1), 85–97.
Ekeroth, F., Kalmteg, N., Pilqvist, J., Runsten, J., 2009. Crosswind Flow Around a High-speed Train on Embankment an Experimental and Numerical Study Bachelor Thesis at Applied Mechanics, The Institution of Applied Mechanics Division of Fluid Mechanics Chalmers university of technology Gothenburg, Sweden. Bachelor Thesis. 2009: TMEX02-09-2.
EN 14067-1, 2003. Railway Applications – Aerodynamics – Part 1: Symbols and units. CEN, Brussels.
EN 14067-6, 2010. Railway Applications – Aerodynamics – Part 6: Requirements and Test Procedures for Cross Wind Assessment. CEN, Brussels.
ESDU Item No. 80024, 1980. Blockage Corrections for Bluff Bodies in Confined Flows, Engineering Sciences Data Unit, London.
Peng H., Xiaodong P., 2010. Embankment wind velocity field and traffic safety under the influence of sudden cross-wind. In: Third IEEE International Conference on Computer Science and Information Technology (ICCSIT). 9–11 July 2010.
Schober, M., Weise, M., Orellano, A., Deeg, P., Wetzel, W., 2010. Wind tunnel investigation of an ICE 3 endcar on three standard ground scenarios. J. Wind Eng. Ind. Aerodyn. 98 (6-7), 345–352.
Sesma, I., Vinolas, J., San Emeterio, A., Gimenez, J.G., 2012. A comparison of crosswind calculations using a full vehicle and a simplified 2D model. Proc. Inst. Mech. Eng. Part F J. Rail Rapid Transit 226 (3), 305–317.
Suzuki, M., Tanemoto, K., Maeda, T., 2003. Aerodynamic characteristics of train/vehicles under cross winds. J. Wind Eng. Ind. Aerodyn. 91 (1-2), 209–218.
Tomasini, G., Cheli, F., 2013. Admittance function to evaluate aerodynamic loads on vehicles: experimental data and numerical model. J. Fluids Struct. 38, 92–106, http://dx.doi.org/10.1016/j.jfluidstructs.2012.12.009.
TSI HS RST, 2008. Technical specification for interoperability relating to the 'rolling stock' sub-system of the trans-European high-speed rail system, section 4.2.6.3. Crosswind, Directive 2008/232/CE, Official Journal of the European Union L847132, pp. 193–195, 2008.